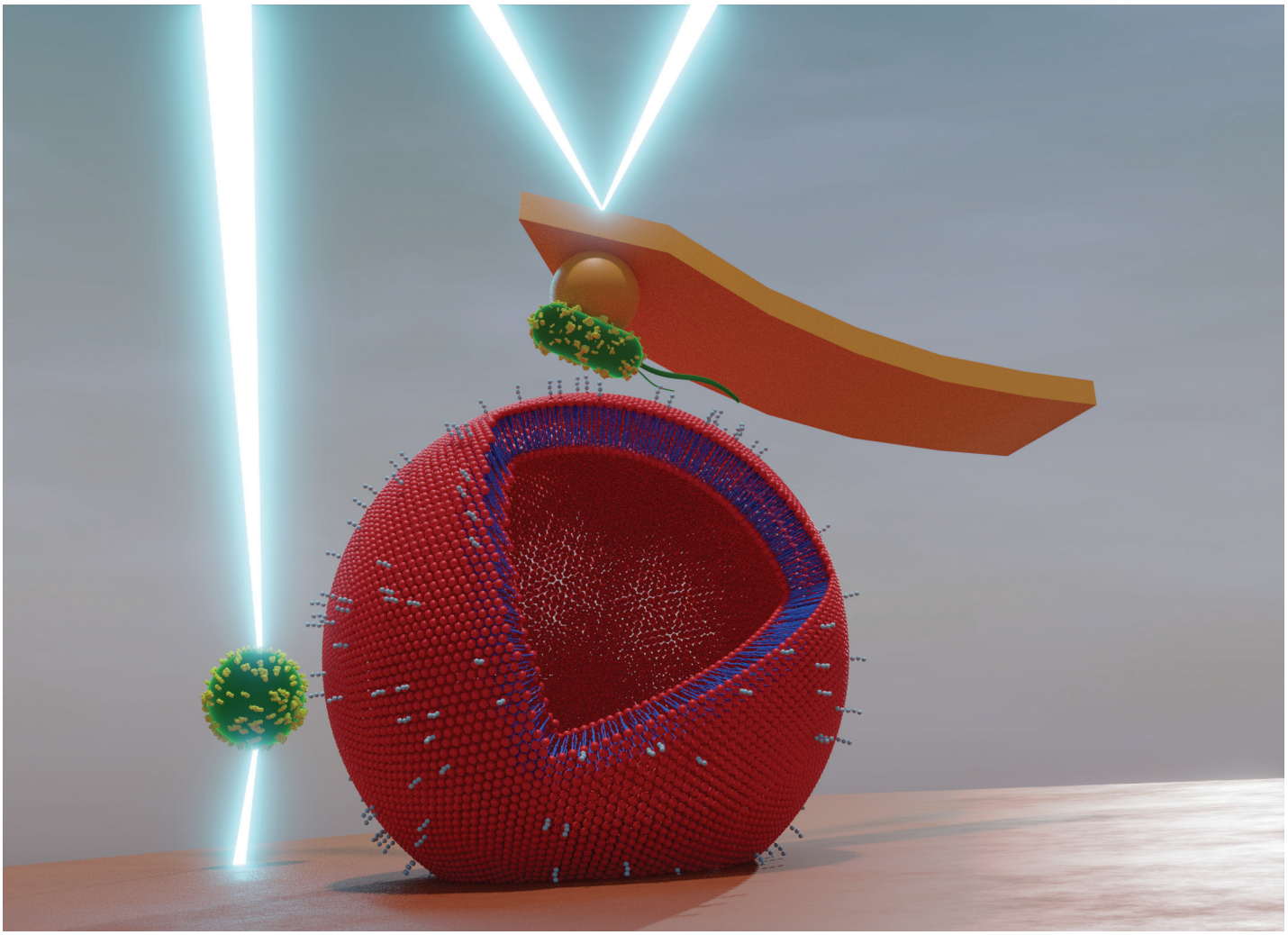

Showcasing research from Professor Römer's laboratory, Signalling Research Centres BIOSS and CIBSS, Faculty of Biology, University of Freiburg, Germany.

Quantification of nanoscale forces in lectin-mediated bacterial attachment and uptake into giant liposomes

The Römer lab investigates host–pathogen interactions and in particular the impact of bacterial lectins on host cell physiology down to molecular detail, by using combinations of analytical and synthetic approaches. In this collaborative project with the Rohrbach lab, IMTEK Freiburg, they quantified nanoscale forces during bacterial attachment and uptake, which arise from the interaction of the Pseudomonas aeruginosa lectin LecA with the host cell glycosphingolipid Gb3 using atomic force microscopy and optical tweezers in combination with giant liposomes.

As featured in:

See Ramin Omidvar, Alexander Rohrbach, Winfried Römer *et al.*, *Nanoscale*, 2021, **13**, 4016.

ROYAL SOCIETY OF CHEMISTRY

rsc.li/nanoscale

Registered charity number: 207890

Nanoscale

PAPER

View Article Online
View Journal | View Issue

Cite this: *Nanoscale*, 2021, **13**, 4016

Quantification of nanoscale forces in lectin-mediated bacterial attachment and uptake into giant liposomes†

Ramin Omidvar, *[a,b,c] Yareni A. Ayala,[d] Annette Brandel,[a,b] Lukas Hasenclever,[a,b] Martin Helmstädter, [e] Alexander Rohrbach,*[d] Winfried Römer *[a,b,c] and Josef Madl ‡[a,b,c]

Interactions of the bacterial lectin LecA with the host cells glycosphingolipid Gb3 have been shown to be crucial for the cellular uptake of the bacterium *Pseudomonas aeruginosa*. LecA-induced Gb3 clustering, referred to as lipid zipper mechanism, leads to full membrane engulfment of the bacterium. Here, we aim for a nanoscale force characterization of this mechanism using two complementary force probing techniques, atomic force microscopy (AFM) and optical tweezers (OT). The LecA–Gb3 interactions are reconstituted using giant unilamellar vesicles (GUVs), a well-controlled minimal system mimicking the plasma membrane and nanoscale forces between either bacteria (PAO1 wild-type and LecA-deletion mutant strains) or LecA-coated probes (as minimal, synthetic bacterial model) and vesicles are measured. LecA–Gb3 interactions strengthen the bacterial attachment to the membrane (1.5–8-fold) depending on the membrane tension and the applied technique. Moreover, significantly less energy (reduction up to 80%) is required for the full uptake of LecA-coated beads into Gb3-functionalized vesicles. This quantitative approach highlights that lectin–glycolipid interactions provide adequate forces and energies to drive bacterial attachment and uptake.

Received 28th October 2020,
Accepted 12th January 2021

DOI: 10.1039/d0nr07726g

rsc.li/nanoscale

1. Introduction

Cell membranes have a highly complex composition of proteins and lipids, which frequently hampers the full characterization of cellular processes. With defined membrane constituents, synthetic membrane systems reduce the complexity of native membranes.[1–3] As a minimal membrane model, giant unilamellar vesicles (GUVs) are well-accepted and widely used to reconstitute diverse cellular processes, such as cell adhesion or endocytosis.[3–7]

The internalization of plasma membrane components, extracellular substances or even pathogens is often mediated by the recruitment of endocytic coat proteins[8] or clustering of glycosphingolipids (GSLs),[9–12] which then induces membrane curvature. Membrane bending/budding mediated by endocytic coat proteins of the classical clathrin-dependent endocytic pathway has been successfully rebuilt in GUVs.[13–15] Upon binding of different bacterial toxins and viruses, the formation of microdomains[12,16] or tubular membrane invaginations[12,17,18] was observed in GUVs enriched in GSLs. Also for bacteria, the binding of lectins to GSLs can be important for membrane bending, for example in lipid-mediated uptake of *Pseudomonas aeruginosa* (PA), referred to as lipid zipper mechanism. Here, the interaction of LecA, a lectin localized at the outer bacterial membrane,[19] with the host cell GSL globotriaosylceramide (Gb3) is sufficient to cause negative membrane curvature and even engulfment of PA in GUVs.[20] The molecular LecA–Gb3 interaction is crucial, since LecA deletion resulted in a significant reduction (about 45%) of PA engulfment in Gb3-functionalized GUVs and also led to significantly less cellular invasion (60% reduction).[20] Furthermore, a direct inhibition of LecA–Gb3 binding by a divalent glycomimetic used in nanomolar

[a]*Faculty of Biology, University of Freiburg, Schänzlestraße 1, 79104 Freiburg, Germany. E-mail: ramin.omidvar@bioss.uni-freiburg.de, winfried.roemer@bioss.uni-freiburg.de*
[b]*Signalling Research Centres BIOSS and CIBSS, University of Freiburg, Schänzlestraße 18, 79104 Freiburg, Germany*
[c]*Freiburg Center for Interactive Materials and Bioinspired Technologies (FIT), University of Freiburg, Georges-Köhler-Allee 105, 79110 Freiburg, Germany*
[d]*Department of Microsystems Engineering (IMTEK), University of Freiburg, Georges-Köhler-Allee 105, 79110 Freiburg, Germany. E-mail: rohrbach@imtek.uni-freiburg.de*
[e]*Renal Division, Department of Medicine, University Hospital Freiburg, Freiburg University Faculty of Medicine, Freiburg, Germany*

†Electronic supplementary information (ESI) available. See DOI: 10.1039/d0nr07726g

‡Current address: Institute for Experimental Cardiovascular Medicine, University Heart Center Freiburg · Bad Krozingen, and Faculty of Medicine, University of Freiburg, Freiburg, Germany.

concentrations resulted in up to 90% reduction in host cell invasion by PA.[21] These findings highlight the importance of LecA–Gb3 interactions in PA pathogenicity.

The lipid zipper mechanism implies that lectin–GSL interactions generate adequate mechanical forces and energies to favor bacterial attachment and to induce membrane curvature to facilitate bacterial internalization into cells. A quantitative (nano-)mechanical analysis of lectin–GSL interactions will provide a deeper understanding of this concept. So far, with regard to interactions of bacteria with surfaces or cells, the generated forces and mechanical properties of PA type IV pili and the flagellum as bacterial attachment factors have been mainly studied.[22–27] The measurement of distinct lectin–carbohydrate interaction forces in presence of other attachment factors (such as protrusive pili, adhesins) or host receptors (various glycolipids and glycoproteins) with higher affinity (*i.e.* higher forces) is technically extremely challenging. In addition, lectins are known to bind to multiple and different glycoconjugates, termed as heterovalency.[28,29] Thus, a controllable membrane composition, *e.g.* as in case of GUVs, is a prerequisite for the direct mechanical quantification of the interaction of interest (LecA–Gb3 binding).

Here, we employed two highly sensitive force probing techniques, atomic force microscopy (AFM) and optical tweezers (OT), in combination with GUVs to analyze in detail the lectin-GSL-mediated pathogen-membrane interaction. In particular, we quantified the LecA–Gb3 interaction forces and energies involved in PA attachment to and engulfment into a membrane model. We used both AFM and OT to study the forces across different regimes of mechanical membrane properties (*i.e.* membrane tension). First, we measured the rather strong interactions of a single, UV-inactivated PA bacterium with Gb3-functionalized GUVs using AFM. Then, the interaction of a minimal, synthetic PA model (LecA-coated AFM tips or OT beads) with GUVs was studied at different membrane tension levels. With AFM, the forces acting on the cantilever were measured while indenting and pulling the membrane of an adherent GUV (Fig. 1A). Using OT, the displacements (and subsequent forces) of LecA-coated beads were measured while a GUV was approached and retracted from the trapped bead (Fig. 1B). Finally, OT permitted tracking the complete uptake of LecA-coated beads into Gb3-functionalized GUVs.

2. Results

2.1 Membrane attachment of the bacterium *P. aeruginosa*

We used AFM-based force probing in combination with fluorescence microscopy to measure the interaction forces between a single PA bacterium, *i.e.* either the PAO1 wild-type strain (PAO1-WT) or the LecA-deletion mutant strain (PAO1-ΔLecA), with Gb3-functionalized GUVs. For biosafety reasons, the bacteria were exposed to UV light for 20 minutes before tip functionalization in order to safely inactivate the pathogenic bacteria. After attaching an inactivated bacterium to a poly-L-lysine-coated colloidal tip (Fig. 2A), the cantilever was transferred without dewetting to another chamber containing GUVs that have been adhered on streptavidin-coated coverslips by incorporation of 1 mol% of biotinylated lipids (Fig. 1A). Two different effective contact times between tips and GUVs were tested: immediate retraction of the AFM tip after indentation, which we termed dwell time 0 s (upper curve in Fig. 2B; left) or retaining the tip-membrane contact for 5 seconds after reaching the setpoint force (dwell time 5 s, lower curve in Fig. 2B; left). During contact period, the *z*-position of the cantilever was kept at constant height.

2.1.1 LecA- and time-dependent attachment of PA to GUVs. We analyzed the detachment force (F_d) by the minimum force in the force–distance (f–d) retraction curve (*i.e.* the maximum negative deviation from the baseline, Fig. 2B; right). In addition, we calculated the detachment work $\left(W_d = \int F dx\right)$, which is integrated along the f–d retraction curve from $d = 0$ to a distance at which full tip-membrane detachment occurs, *i.e.* zero force (grey area in Fig. 2B; right). The pulling velocity in all experiments was 1 μm s^{-1}. For a dwell time of 0 s, the presence of LecA had no profound effect on membrane attachment (Fig. 2C). The average value of the detachment forces for PAO1-ΔLecA (F_d = (104 ± 52) pN) was slightly lower than that for PAO1-WT (F_d = (171 ± 102) pN). The detachment work was averaged to $W_d = (17.0 \times 10^3 \pm 15.7 \times 10^3)\ k_BT$ and $(32.7 \times 10^3 \pm 30.1 \times 10^3)\ k_BT$ for PAO1-ΔLecA and PAO1-WT strains, respectively (Fig. 2D).

Interestingly, the PAO1-ΔLecA and PAO1-WT strains showed different effects when they were kept in contact with GUV membranes for some seconds. Changing the dwell time from 0 s to 5 s resulted in significant increases in detachment force and work for PAO1-WT in contrast to PAO1-ΔLecA, which remained largely unaffected. The average values of the detachment forces were measured as F_d = (122 ± 37) pN and (507 ± 55) pN for PAO1-ΔLecA and PAO1-WT groups, respectively (Fig. 2C). The detachment work increased from $W_d = (20.2 \times 10^3 \pm 10.5 \times 10^3)\ k_BT$ for PAO1-ΔLecA to $W_d = (187.1 \times 10^3 \pm 28.1 \times 10^3)\ k_BT$ for PAO1-WT bacteria (Fig. 2D).

The 5.8-fold increase in detachment work for PAO1-WT (from 0 s to 5 s dwell time condition; box plots of W_d graphs for PAO1-WT in Fig. 2D) indicates that LecA can distinctly reinforce the PA attachment to the membranes in a relatively short time window. The reinforcement can be explained as Gb3 lipids from the non-contact area can diffuse into the contact region and bind to unoccupied LecA binding pockets, which effectively results in the increased Gb3 density and stronger interaction.

2.1.2 Higher unbinding forces and pulling lengths for wild-type bacteria. After surpassing a certain force threshold (F_d), a force–distance curve typically continues with step-like events, which are attributed to the rupture of adhesive units (here the lectin LecA and the glycosphingolipid Gb3). The position (from zero distance; referred to as pulling length) and relative height (unbinding force) of each unbinding step (Fig. 2B; right) were further computed from f–d curves with 5 s of dwell time (Experimental section and Fig. 2E & F). The number of unbinding events for PAO1-WT bacteria was signifi-

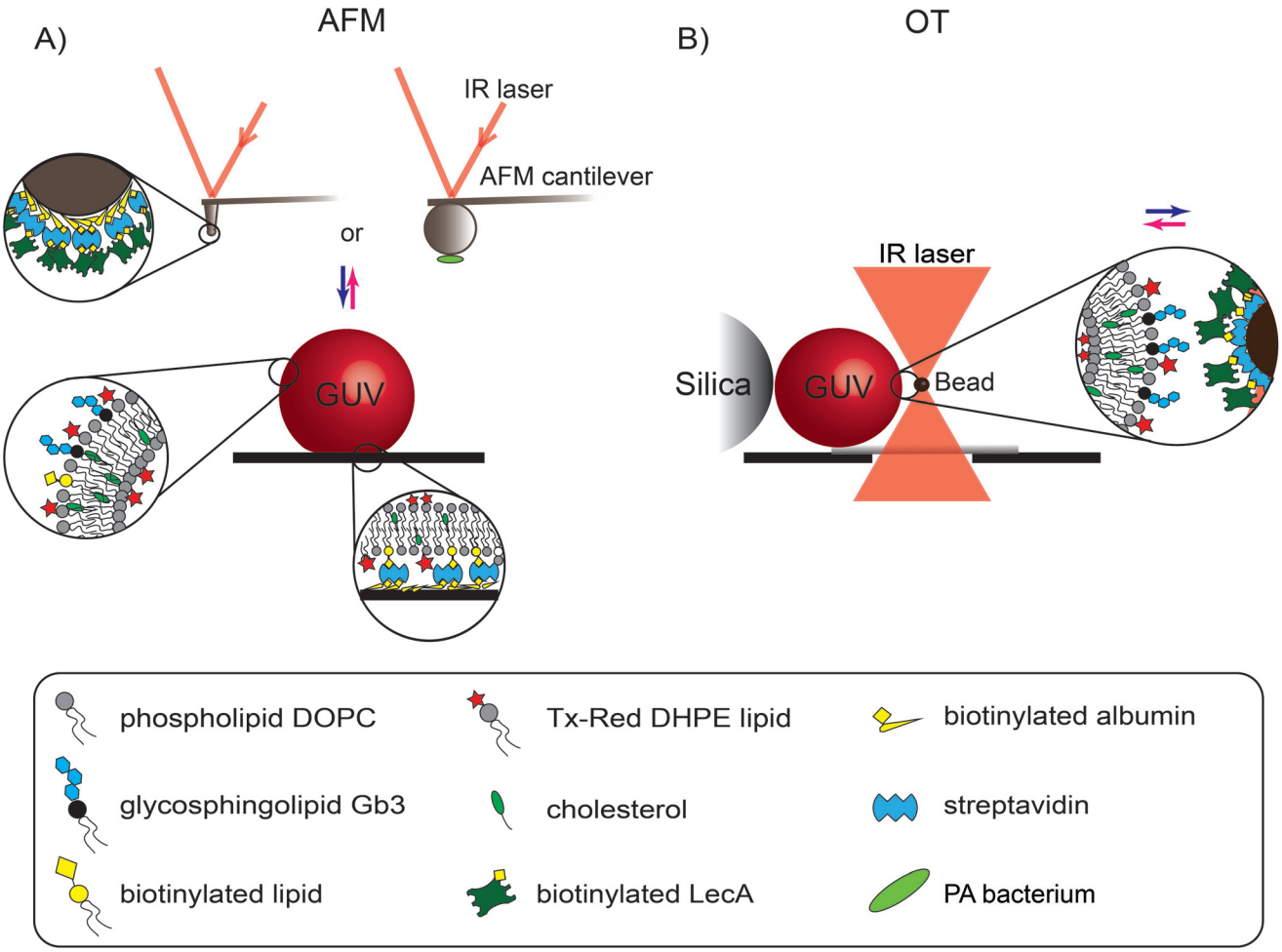

Fig. 1 Schematic illustration of the applied experimental techniques for the force quantification of bacterial attachment to and engulfment into a giant unilamellar vesicle: (A) atomic force microscopy (AFM) and (B) optical tweezers (OT). Giant unilamellar vesicles (GUVs) were adhered for AFM measurements using biotin–streptavidin linkage. The movement of GUVs in the OT setup was constrained by a silica bead. The changes in the deflection of the AFM tip or the displacement of the OT bead were recorded by an infrared (IR) laser detection system and then converted to force. The scheme is not drawn to scale.

cantly higher than for the PAO1-ΔLecA strain. The unbinding forces covered much higher values demonstrating increased affinity when LecA is present on the surface of the bacterium. For the PAO1-WT strain, two peaks could be possibly conjectured. The lower peak at ~30 pN was closer to the peak of PAO1-ΔLecA strain (24 pN) probably representing non-specific interactions, while the higher peak at about ~70 pN originates from specific LecA–Gb3 unbinding events. The average pulling length of steps was shifted about 2 μm showing the prolonged adhesion of PAO1-WT bacteria due to LecA binding to Gb3 (Fig. 2F).

2.2 Interactions of LecA-coated AFM tips mimicking a minimal, synthetic PA with membranes

As a consequence of LecA–Gb3 binding, PAO1-WT builds up a strong attachment to the membrane within seconds. Until today, LecA is the only identified ligand of PA that binds to Gb3 lipids.[30] In the previous section, the LecA-deletion mutant strain confirmed that the interaction of PA with a Gb3-functionalized GUV is significantly reduced in the absence of LecA. However, to completely abolish the possible influence of other proteins or lipids of PA in the attachment process, we designed a synthetic, minimal model of PA using functionalized AFM tips. A tip with an 800 nm diameter hemisphere (Fig. 3A) was coated with biotinylated LecA (0.1 mg ml^{-1}; Fig. 1A). Tip functionalization was performed *via* biotin–streptavidin linkage to assure that LecA stays attached to the tip in the course of the experiment due to the very high affinity of biotin–streptavidin ($K_d \approx 10^{-15}$ M (ref. 31)) compared to medium-range affinity of LecA–Gb3 ($K_d = 77 \times 10^{-6}$ M (ref. 32)). As control group, tips were only coated with bovine serum albumin.

2.2.1 Increased detachment forces and works between LecA-coated tips and Gb3-functionalized GUVs. GUVs containing Gb3 (GUV^+) or GUVs without Gb3 (GUV^-) exhibited non-specific interactions with albumin-coated tips (Fig. 3B). The average value of detachment forces between albumin-coated

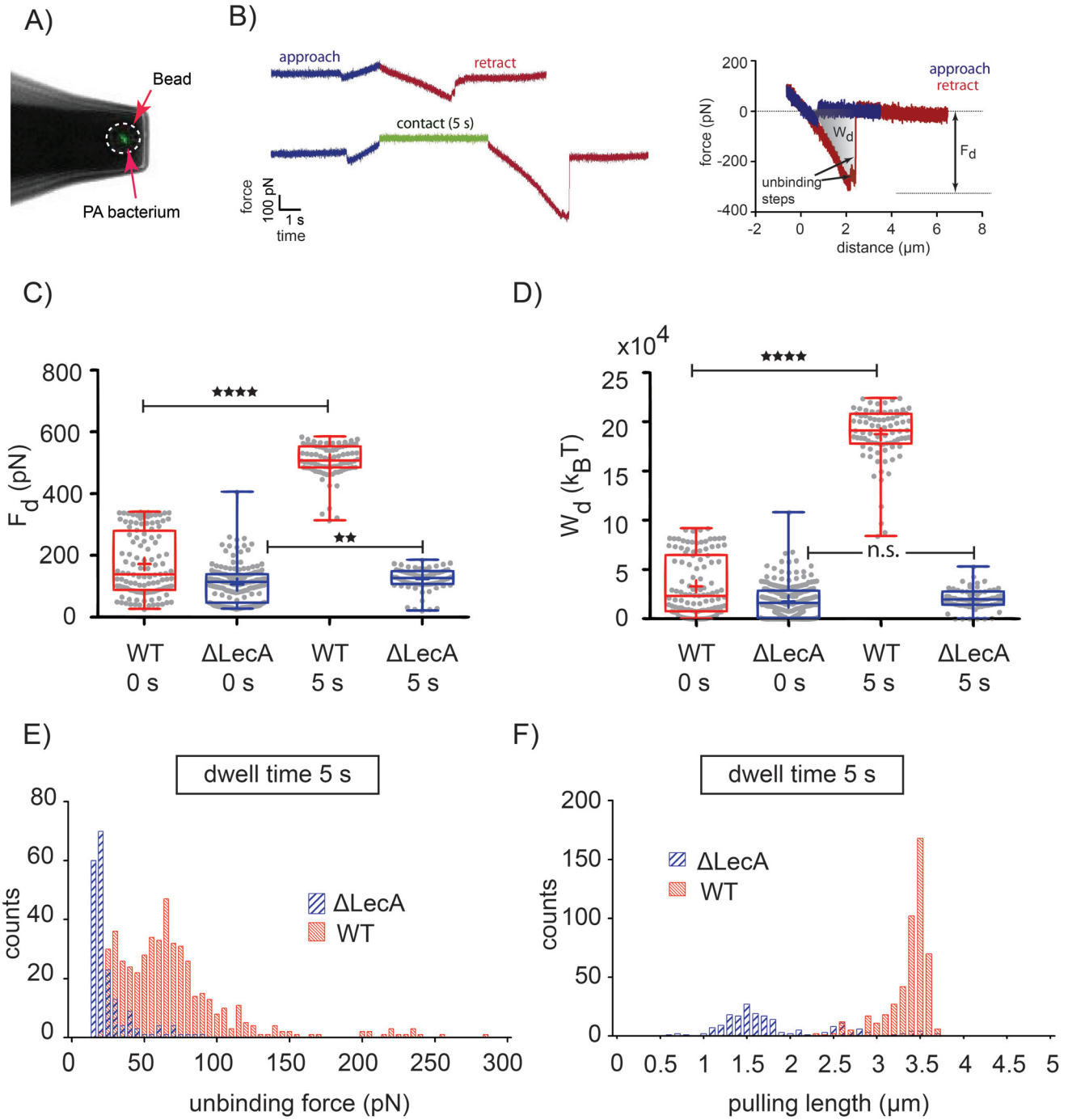

Fig. 2 LecA- and time-dependent membrane attachment of *Pseudomonas aeruginosa*. (A) An inactivated GFP-tagged bacterium was attached to the poly-L-lysin-coated colloidal (*i.e.* bead) tip (overlay fluorescence/bright field). (B) (Left) Representative force–time curve depicts the dwell time of (upper) 0 s and (lower) 5 s. (Right) A representative force–distance curve represents the detachment force, detachment work and unbinding steps. Comparisons of (C) the detachment force (F_d) and (D) the detachment work (W_d) between WT (PAO1-WT) and LecA-deletion (PAO1-ΔLecA) PA strains for 0 s and 5 s of dwell time; the total number of acquired curves for PAO1-WT and PAO1-ΔLecA was 205 and 295, respectively. ****: *P*-Value < 0.0001 using Mann–Whitney-*U*-test; mean values were marked with a plus sign. Analysis of single unbinding steps showed the frequency distributions of (E) unbinding forces and (F) pulling lengths for the dwell time of 5 s.

tips and GUVs did not significantly depend on the presence of Gb3 (F_d = (56 ± 37) pN for GUV^-, F_d = (76 ± 54) pN for GUV^+; Fig. 3C). Detachment work displayed only a slight change (Fig. 3D; W_d = $(2.4 \times 10^3 \pm 3.9 \times 10^3)$ k_BT for GUV^- and $(3.2 \times 10^3 \pm 2.3 \times 10^3)$ k_BT for GUV^+, respectively). In the case of LecA-coated tips, mainly two types of curves were recorded, *i.e.* curves with multiple unbinding events or curves with high detachment forces (Fig. 3B). About 20% of recorded curves

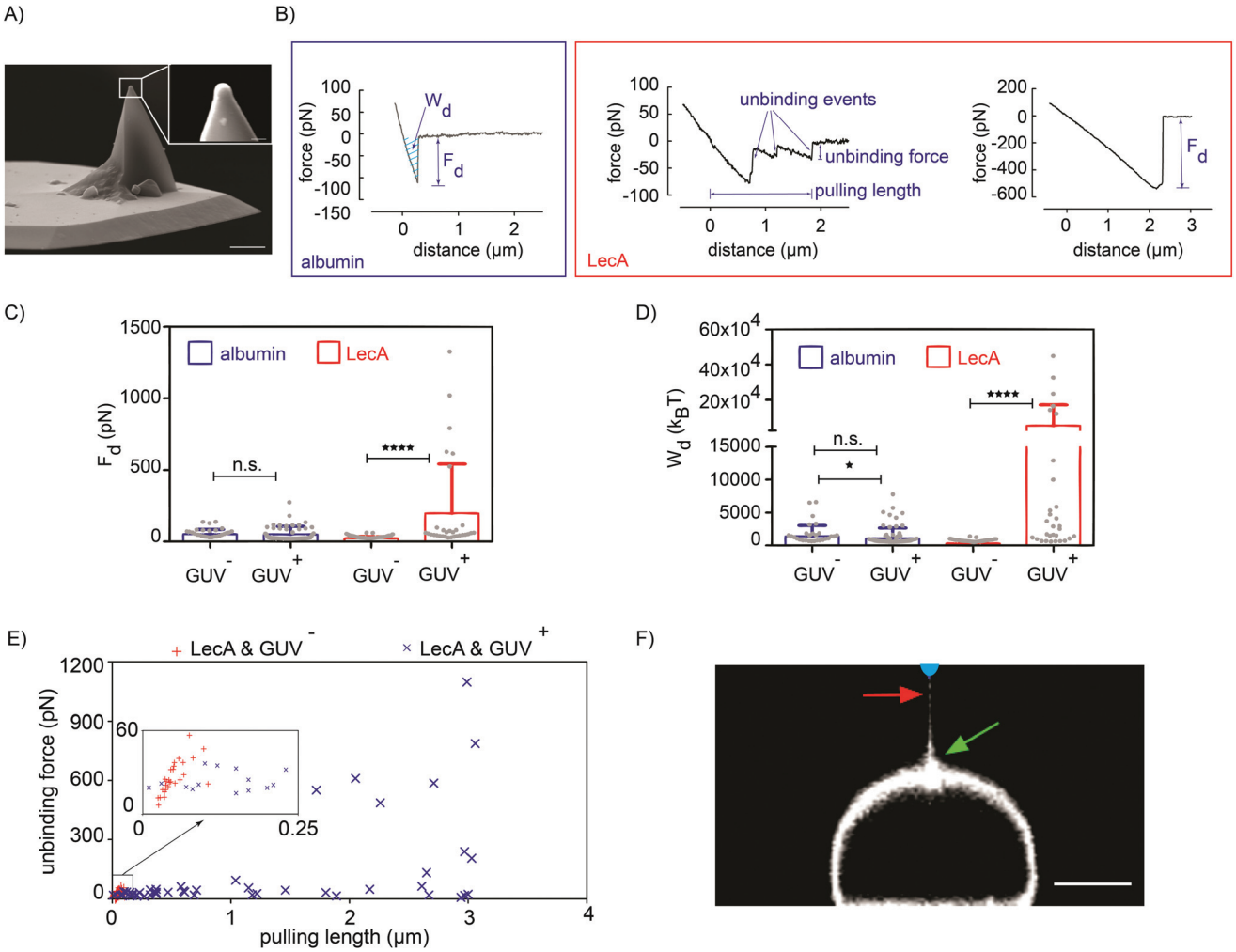

Fig. 3 Strong attachment, high unbinding steps and pulled membrane tethers between LecA-coated AFM tips and Gb3-functionalized GUVs. (A) A SEM image of the used AFM tips (scale bar: 9 μm) shows a pyramid tip with a hemisphere end which is of similar size to a PA bacterium (scale bar in zoomed area: 900 nm). (B) Representative *f–d* curves for albumin-coated tips (blue box) and LecA-coated tips (red box) and analyzed parameters: detachment force (F_d), detachment work (W_d), the height (unbinding force) and position (pulling length) of unbinding steps. Comparison of (C) the detachment force and (D) the detachment work for albumin- and LecA-coated tips interacting with Gb3-positive GUVs (GUV^+) or Gb3-negative GUVs (GUV^-). Presence of LecA on tips and Gb3 in the GUV membrane led to a significant increase in detachment force and work (the total number of curves for albumin- and LecA-coated tips is 85 and 60, respectively; ****: *P*-Value < 0.0001 using Mann–Whitney-*U*-test). (E) The unbinding force *versus* pulling length graph for LecA-coated tips interacting with GUV^- and GUV^+ vesicles. Zoomed area in (E) illustrates the unbinding steps with lower pulling length (<250 nm). (F) Membrane deformation of a GUV during retraction of LecA-coated tips recorded as z-stack with a confocal microscope. Green and red arrows point to the catenoid shape and membrane tether formation, respectively. The blue hemisphere indicates the tip position (scale bar: 5 μm).

showed high detachment forces (from 530 pN to 1377 pN) and were similar to *f–d* curves of the AFM assay with PAO1-WT bacteria (dwell time 5 s condition; Fig. 2B). Based on these curves for LecA-coated tips, the average value of detachment forces for GUV^+ was about 8-fold higher than that for GUV^- (Fig. 3C). Not only showing higher detachment force values, the full detachment occurred at much higher pulling lengths ((2.60 ± 0.43) μm) compared to the other conditions (*e.g.* (0.05 ± 0.02) μm for LecA/GUV^-). This resulted in a strong increase of the average value of detachment work for the LecA/GUV^+ condition compared to LecA/GUV^- (about 170-fold; Fig. 3D). For the LecA/GUV^+ condition, we often observed that a signal from the fluorescent membrane marker appeared on the tips after several force–distance cycles. Since tip-attached lipids might non-specifically cover LecA or even block LecA binding pockets, which both result in undesired interactions, the fluorescence signal on the AFM tip was monitored after each recorded curve to check for lipid contaminations (Fig. S1†). The lipid contamination limited us to dwell time 0 s.

2.2.2 Higher unbinding forces and pulling lengths as a result of LecA–Gb3 binding. For Gb3-negative GUVs (GUV^-), all unbinding events happened within the first 450 nm of the retraction – regardless of the tip functionalization (Fig. 3E for LecA-coated tips and Fig. S2A† for albumin-coated tips). In the

case of LecA-functionalized tips and Gb3-positive GUVs (GUV^+) (Fig. 3E), we observed unbinding steps with different unbinding force values (<1.1 nN) in a broad range of pulling lengths (from 12 nm to 3.06 μm; Fig. 3E). The higher unbinding forces for LecA/GUV^+ are due to the rupture of several LecA–Gb3 non-covalent bonds. Dividing the pulling lengths by the constant velocity of the retracting cantilever transforms the length to bond lifetime.[33] Increased pulling lengths for LecA/GUV^+ might point to an increased lifetime of PA–membrane interactions, which favors PA colonization and host cell infection. For albumin-coated cantilevers and GUV^+, unbinding forces above 150 pN were never observed (Fig. S2B†).

2.2.3 LecA-coated tip pulls long tethers out of the membrane. Recorded z-stack images from a combined AFM and confocal laser scanning microscopy (CLSM) system exhibited the formation of a funnel-like shape (catenoid) of the membrane (green arrow in Fig. 3F) followed by a long membrane tether outward from the GUV^+ (red arrow in Fig. 3F). Membrane tether formation can be recognized in *f–d* curves through the presence of a long plateau with a constant force before the unbinding step.[34,35] This characteristic feature was only observed for increased LecA coverage on the AFM tips (by doubling the LecA solution concentration from 0.1 to 0.2 mg ml^{-1}; Fig. S3A†). As stated for increased pulling lengths, the outward tethers imply that LecA–Gb3 interactions might substantially increase the PA–membrane interactions. Similar to the lower LecA concentration (0.1 mg ml^{-1}), curves with high detachment forces (21% of curves; Fig. S3B†) were recorded for 0.2 mg ml^{-1} LecA.

2.3 Interactions of LecA-coated OT beads representing a minimal, synthetic model of the PA bacterium with membranes

By AFM quantification of forces and energies, which are required to detach a single bacterium or a LecA-coated tip as minimal bacterial model from Gb3-functionalized membranes, we deduce that LecA–Gb3 interactions result in stronger attachment of PA to the membrane in a time-dependent manner. Reduced membrane tension adjustment[36] in artificial membrane systems like GUVs, due to missing cellular membrane reservoirs, results in larger in-plane tension (pre-stress), especially in adherent GUVs compared to cells.[37] Non-adherent GUVs possess lower tension than adherent GUVs and can be more relevant to cellular membrane native conditions with regard to membrane tension. Thus, another probing technique with high force resolution, optical tweezers (OT), was employed to examine LecA–Gb3 interactions in non-adherent GUVs, while constraining their displacements upon the optical forces with large silica beads. Moreover, OT are capable of measuring forces of a few piconewtons and below, which are within the typical noise level of AFM. A nanometer-precise 3D control of the OT bead movement allows to bring the bead in the close vicinity of the membrane and to measure small force changes during initial attachment. Streptavidin latex beads (1 μm) were coated with biotinylated LecA to interact with two groups of vesicles (GUV^- and GUV^+). LecA coverage of the beads was confirmed by fluorescence microscopy (Fig. S4†). Streptavidin-coated beads have been used as control group. Using a piezoelectric stage, a selected GUV was moved towards the optically trapped LecA-coated bead and pressed against the bead for a few seconds before the GUV was moved away.

2.3.1 Increased attachment rate and detachment forces due to LecA–Gb3 binding. Fig. 4A illustrates different interaction cases and the subsequent interaction steps (I–VIII). In some cases, no attachment between the bead and the GUV was observed (0) "No Adhesion" case (Fig. 4A). However, when we observed adhesion, three different interaction courses could be distinguished during retraction: (1) Adhesion-no detachment: in this case, the strength of the attained adhesion overcame the optical trapping force, which was neither strong enough to detach the bead from the membrane nor to produce any large membrane deformation. Therefore, the bead was pulled out from the optical trap (VIII: empty trap) and remained adherent to the vesicle surface (Fig. 4A). (2) Adhesion-tether: Here, unlike the previous case, the membrane was deformed following the catenoid-tube equilibrium shape transition (step II in Fig. 4A). However, the particle did not detach from the membrane during the retraction part and a long membrane tube (tether) was formed between the bead and the GUV (step IV). (3) Adhesion-detachment: In this case, the membrane abruptly detached from the bead, which remained trapped by the laser (step VI in Fig. 4A).

The disruption occurred either during the formation of the catenoid or after the tether extension. The detachment force was measured only from the Adhesion-detachment events. The presence of Gb3 and LecA led to a higher probability of adhesion events (more than 80%, from a total of 102 experiments; see stacked bar graph for LecA/GUV^+ condition in Fig. 4B). The frequency of adhesion cases dropped to 41% when neither LecA nor Gb3 were present (total number of experiments 51; stacked bar graph for streptavidin/GUV^- condition in Fig. 4B). Similar to AFM results, we measured higher detachment forces for the LecA/GUV^+ group (average value: F_d = (10.1 ± 2.6) pN as shown in Fig. 4C). When both LecA and Gb3 were absent, the detachment force was computed as F_d = (6.9 ± 2.6) pN (streptavidin/GUV^- in Fig. 4C). For other groups, *i.e.* LecA/GUV^- and streptavidin/GUV^+, the average detachment forces were measured as F_d = (7.2 ± 3.3) pN and F_d = (7.2 ± 5.9) pN, respectively (Fig. 4C). These results showed that in non-adherent GUVs with lower in-plane tension than adherent GUVs and with lower applied forces (<20 pN) compared to AFM (>50 pN), LecA–Gb3 interactions still increase the detachment of LecA-coated beads as minimal bacterial model from GUVs (about 1.5 fold).

2.4 Engulfment of LecA-coated beads into GUVs

In the previous sections, pulling experiments with AFM and OT demonstrated that LecA–Gb3 interactions reinforce the attachment of the bacterium to the membrane, which is the first step of bacterial uptake. However, the experimental quantification of the impact of LecA–Gb3 interactions on bac-

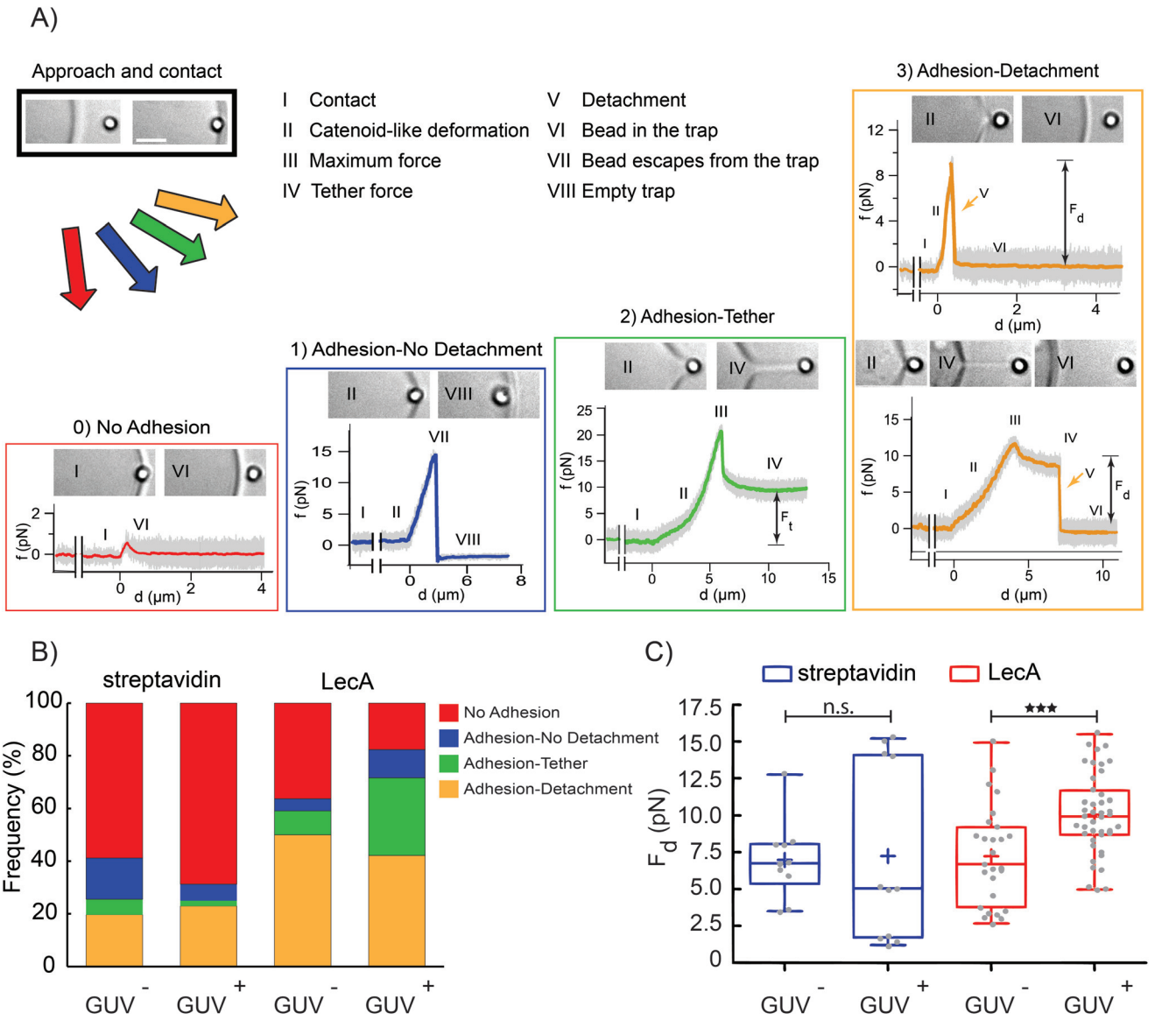

Fig. 4 Increased attachment probability and detachment forces for LecA-coated OT beads indenting Gb3-functionalized GUVs. (A) After establishment of contact between the streptavidin- or LecA-coated beads and GUVs (approach and contact box, scale bar: 2 μm), the GUV was moved away from the bead and different cases of interactions between beads and GUVs were observed and classified as: (0) No adhesion, (1) adhesion-no detachment, (2) adhesion-tether and (3) adhesion-detachment. I–VIII. Bright field images showed specific stages qualitatively, force–distance (f–d) profiles allowed quantitative characterization. (B) Frequency of observation of the above-mentioned events for different test groups: streptavidin-coated beads (as control; 51 experiments) and LecA-coated beads (102 experiments) interacting with GUV^- and GUV^+. (C) The detachment force (F_d) for different test groups (the total number of curves used for F_d calculation is 70 and 21 for LecA- and streptavidin-coated beads, respectively; ***: P-value < 0.001 using Mann–Whitney-U-test, average values were marked with a plus sign).

terial engulfment still remains unanswered. Unlike AFM, OT can provide a complete internalization of the probe into GUVs, thereby mimicking the bacterial uptake process. In a previous work, a photonic force microscope (PFM) was used to study how uptake forces and energies are related to changes in the bead's position fluctuations, which encode stiffness and viscous drag of the GUV membrane during bead uptake.[38]

Here, we used OT to drive LecA-coated beads into Gb3-functionalized vesicles to further investigate the influence of LecA–Gb3 interactions on the forces and energies of the uptake process. As a control, we used DOPC vesicles indented with pure latex beads, on which LecA was not present.

2.4.1 GUV elasticity defines the deformation energy profile during uptake. After the initial bead-membrane contact, the membrane was indented further to progressively wrap the bead. We defined a complete internalization of the bead when a membrane tether formation inside the GUV could be recognized in force–distance curves. The force–distance curves (Fig. 5A) presented a sharp increase in the force starting at d = 0 (bead is in contact with the membrane) until it reached a

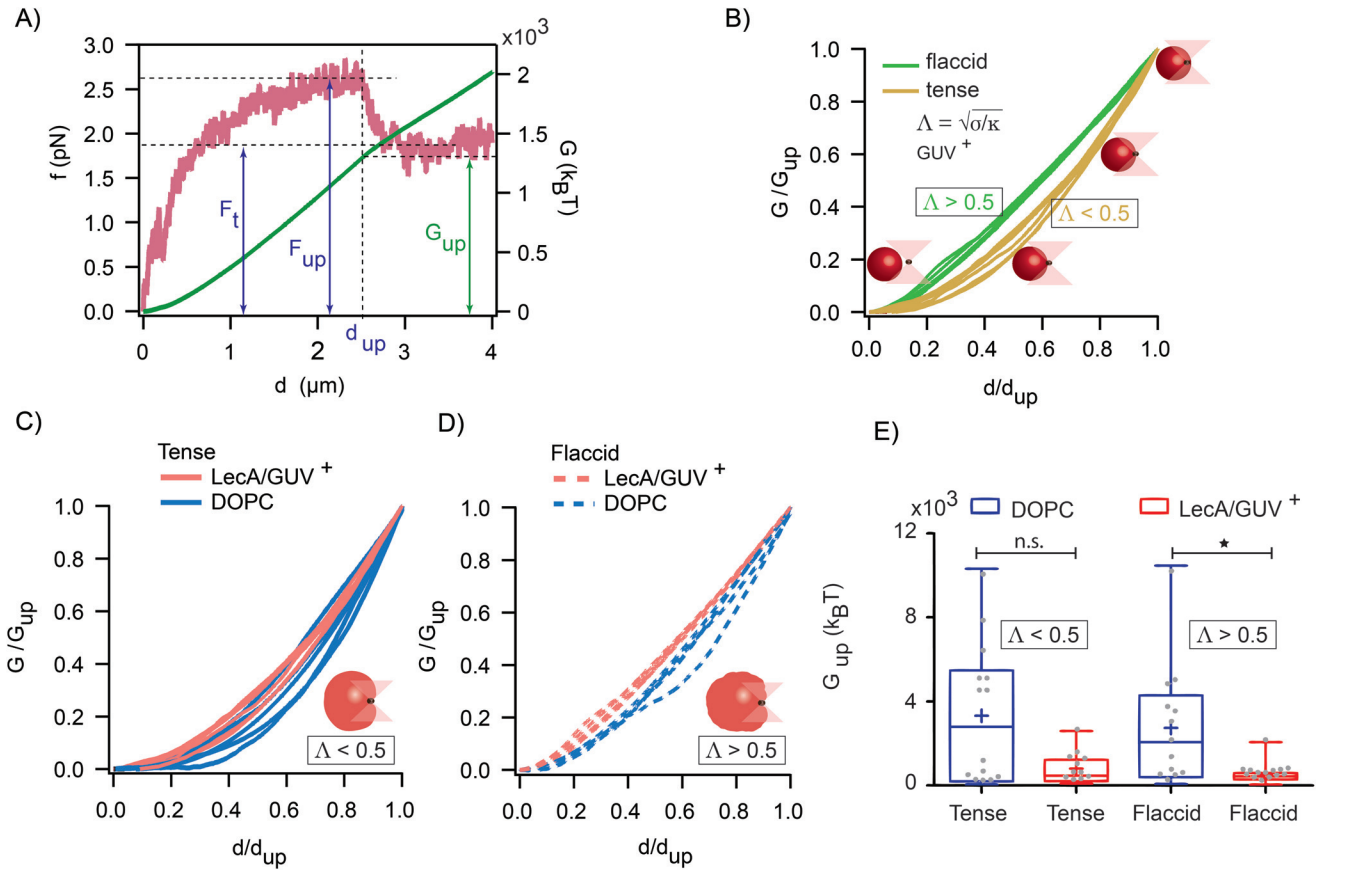

Fig. 5 Different deformation energy profiles and reduced uptake energy as the result of LecA–Gb3 interactions (A) A representative force–distance (f–d) curve (red) depicts the required force (F_{up}) and energy (G_{up}) for the internalization of the bead into the GUV at the distance (d_{up}). The tether force (F_t) was used to determine the mechanical properties of the membrane. The energy profile (green curve) was obtained by integrating the force (f) over the distance (d) and used to compute the uptake energy (G_{up}). (B) Normalized energy-distance curves for tense (gold) and flaccid (green) vesicles with similar size. Comparison of the energy profiles between DOPC vesicles and (C) tense or (D) flaccid Gb3-functionalized vesicles. (E) The average uptake energy demonstrated a reduction for the case of LecA–Gb3 interactions in both tense and flaccid vesicles (the total number of uptake experiments for DOPC and GUV$^+$ vesicles are 27 and 26, respectively; *: P-value < 0.05 using Mann–Whitney-U-test, average values were marked with a plus sign).

maximum value (F_{up}) at $d = d_{up}$ (distance at which uptake occurs). As theoretically modelled in ref. 20, the LecA–Gb3 interactions add a curvature-promoting energy term during the indentation stage ($d = 0$ to $d = d_{up}$). At $d = d_{up}$, the bead reached a maximum degree of membrane wrapping and the force dropped to a constant value (F_t; termed as tether force), which corresponds to the tether formation inside the GUV.

The maximum value of the force (F_{up}) represents the required force to overcome the mechanical barrier, which is imposed by the membrane elasticity. The energy profile, which is computed from the integral of the force–distance curve ($G = \int F\mathrm{d}x$), is depicted in Fig. 5A. The tether force (F_t) and the tether radius (R_t) measured from fluorescence microscopy images were used to calculate the membrane tension (σ) and bending rigidity (κ) of the vesicles.[39,40] We used the intrinsic length scale Λ ($\Lambda^2 = \frac{\kappa}{\sigma}$) parameter, representing the interplay between stretching and bending energies,[39,41] to sort GUVs in two groups depending on the membrane mechanical state: tense and flaccid vesicles. By comparing GUVs with similar Λ, we minimized any additional influence in the uptake process due to the differences in their elastic properties.

The global and local response of the membranes to the indenting force can be better visualized using the normalized energy profiles.[38] For the tense (Λ < 0.5 μm) and flaccid (Λ > 0.5 μm) GUVs with similar size (radius ~9 μm), we normalized the energy profiles by their corresponding values of G_{up} and d_{up} (Fig. 5B). We observed that the deformation energy curves for flaccid GUV$^+$ exhibited a linear-like growing throughout the uptake process, while for tense GUV$^+$ the energy profiles showed a slower growth at the onset of indentation process followed by a steeper increase in the energy.

2.4.2 LecA–Gb3 binding reduces required energy for bead engulfment. We compared the energy profiles $G(d/d_{up})$ normalized by G_{up} from GUV$^+$ with those obtained from GUVs solely composed of DOPC using Λ to distinguish between flaccid and tense vesicles (Fig. 5C and D). Interestingly, despite the fact that vesicles with similar membrane elastic properties (Λ) have been compared, differences in the course of the energy curves

could be observed. For the tense vesicles of the LecA/GUV$^+$ group, the energy profiles grew faster than the energy profiles measured from vesicles of the DOPC group (Fig. 5C). Although less noticeable, the same held true for the flaccid vesicles (Fig. 5D). In the framework of local and global deformations, the faster growth of the deformation energy must be attributed mainly to the interactions of LecA with Gb3 and not to differences in the mechanical properties of GUVs.

Moreover, by comparing the average values of the uptake energy (G_{up}) for flaccid and tense GUVs, we observed lower average uptake energy when both LecA and Gb3 were present ($G_{up} = (0.81 \times 10^3 \pm 0.76 \times 10^3)\ k_BT$ for tense and $G_{up} = (0.52 \times 10^3 \pm 0.48 \times 10^3)\ k_BT$ for flaccid GUVs; Fig. 5E).

3. Discussion

3.1 Strong bacterial attachment to membrane increases with LecA–Gb3 interactions and contact time

Nanoscale forces between single inactivated PA bacteria (*i.e.* wild-type and LecA-deletion PAO1 strains) and Gb3-functionalized vesicles were measured. The LecA-deletion mutant of PA bacteria exhibited only low detachment forces both with minimal dwell time but also after 5 s of contact (Fig. 2C). Observing almost no change in the measured forces with increasing dwell time suggests that the host cell glycosphingolipid Gb3 does not interact with any other PA adhesion molecule. In contrast to this, wild-type PA bacteria showed significantly higher detachment forces and works, in particular, after a few seconds of contact. The 6-fold increase in the average value of detachment work between 0 s and 5 s of dwell time might originate from increased local density of Gb3 within the contact region after few seconds, as previously shown by the increased fluorescence intensity of bound LecA between two crosslinked GUVs over time.[6] Comparing the detachment forces (F_d = (507 ± 55) pN) with forces that a single type IV pilus, as an important bacterial motility motor, generated on abiotic surfaces (110 ± 30) pN (ref. 22) or on epithelial cells (70 ± 20) pN (ref. 42) reveals that LecA-induced Gb3 clustering can produce strong forces, which presumably lead to membrane deformation and eventually bacterial engulfment.

The detachment work is comprised of two contributions that are practically impossible to separate: membrane deformation (bending or stretching) and unbinding work of multiple adhesion bonds.[33] However, dividing the detachment works by the adhesion energy of a single LecA–Gb3 bond (5.6 kcal mol^{-1}, equals to ~9.5 k_BT per lipid[32]), a very simplified overestimation of the number of LecA–Gb3 bonds can be calculated. The tetrameric LecA contains four carbohydrate binding pockets at two opposing sides. Assuming one side of LecA binds to a GUV (*i.e.* to 2 Gb3 lipids), the number of GUV-bound LecA becomes half of the number of LecA–Gb3 bonds. Therefore, for WT-PAO1 with 5 s of contact ($W_d = (187.1 \times 10^3 \pm 28.1 \times 10^3)\ k_BT$), the number of LecA can be calculated as $9.84 \times 10^3 \pm 1.47 \times 10^3$. The outer membrane of PA, like for many other Gram-negative bacteria, is covered with bristle-like short fibers termed fimbriae.[43] Several hundreds to thousands of fimbriae are evenly distributed on the bacterial membrane, and they may contain lectins, for example FimH on *Escherichia coli* fimbriae.[43,44] No study has resolved the localization of LecA on the PA outer membrane yet. Considering a dense coverage of the bacterial surface with thousands of fimbriae, the above-estimated number of LecA suggests that LecA resides on fimbriae. It is noteworthy to mention that the measured force–distance curves did not exhibit the characteristic features (*i.e.* force plateau and extended rupture lengths) of retracting type IV pili.[26,27] Thus, we hypothesize that LecA can be located on PA fimbriae, but not on type IV pili.

3.2 Simplistic models of bacterium and host cell prove importance of LecA–Gb3 interactions

The quantifications of the detachment forces and energies revealed that more work is required to detach LecA-coated AFM tips from Gb3-positive vesicles than from Gb3-negative GUVs. Both, increased pulling lengths and formation of membrane tethers in the LecA/GUV$^+$ condition imply that LecA–Gb3 binding strengthens PA–host membrane interactions, thus favoring bacterial colonization and internalization. Albumin-coated probes showed reduced interactions, meaning that they required lower unbinding forces and less detachment works, since they interacted non-specifically with GUVs. Also in the low force regime, *i.e.* using OT with LecA-coated beads, higher detachment forces were observed on Gb3-positive GUVs.

The membrane tension is a crucial physical parameter in many cellular processes, *e.g.* endocytosis or phagocytosis.[45] Here, we illustrate that LecA–Gb3 interactions reinforced the attachment of a minimal bacterial model (*i.e.* LecA-coated tips and beads) independently of the membrane tension level regimes (high lipid bilayer tension in AFM tests (0.1–1 mN m^{-1} (65)) due to substrate attachment and low lipid bilayer tension ($0.40–1.09 \times 10^{-3}$ mN m^{-1}) measured from OT adhesion-tether formation cases (Fig. 4A)).

With the OT setup, it was possible to estimate the probability for observed adhesion (frequency) between LecA-coated beads and GUVs. LecA–Gb3 interactions resulted in almost twice the adhesion frequency compared to the condition where both LecA and Gb3 were absent. In almost 40% of OT pulling experiments, the LecA–Gb3 interactions were even stronger than the optical trapping forces in our experimental setups and consequently, the bead could not be detached from the membrane.

3.3 LecA-driven uptake of bacterial model into GUVs is energetically favorable

During complete internalization of LecA-coated beads into GUVs, different energy profiles were observed for flaccid and tense Gb3-positive GUVs (Fig. 5B). As demonstrated for POPC vesicles in Meinel *et al.*[38] these differences in the energy profiles are due to variations in the mechanical state of their membranes. Briefly speaking, a linear-like growth of the energy is associated to local deformations of the vesicles. Therefore, for a flaccid vesicle, due to the excess of membrane,

the indenting bead can be wrapped without producing major changes in the global shape of the vesicle. On the other hand, in a tense vesicle, the changes in membrane tension propagate rapidly throughout the membrane leading to a global deformation at the beginning of the uptake process (oblate ellipsoid shape), while local deformations take place at later stages. Moreover, in comparison to Gb3-negative GUVs, the uptake energy was reduced by a factor of 4.1 or 5.2 (tense or flaccid, respectively), which indicates that LecA–Gb3 interactions reduce the energetic entry costs through local membrane deformations rather than global changes.

4. Conclusion

The internalization of several pathogenic bacteria such as *Listeria monocytogenes* or *Staphylococcus aureus* over a micrometer sized area of the plasma membrane is mediated by clathrin assembly and establishment of actin meshwork, which are the principal steps of clathrin-mediated endocytosis (CME), classically described for nanometer sized membrane invaginations.[46–48] However, the stored energy in a crosslinked actin meshwork ($\sim 10^4\ k_BT$) was estimated to provide about 1/6 of the total energy needed in CME in yeast.[49] The polymerization energy of clathrin ($\sim 40\ k_BT$ per triskelion[50] and $\sim 500\ k_BT$ in total[51]) also can not directly initiate membrane curvature.[51] Therefore, above-mentioned energies are not plausibly adequate to accomplish bacterial internalization that occurs at a larger scale – albeit epithelial cells possess lower internal pressure (40–400 Pa (ref. 52)) than a yeast cell (~1 MPa (ref. 49,53)), which is the most common model in CME. Hence, other membrane-deforming mechanisms and force generators must be involved, as nicely reviewed in ref. 51. We have previously proposed a lipid-based mechanism for the PA bacterium entry into the non-phagocytic epithelial cells in the absence of actin.[20] The findings of the current study – increased attachment forces (1.5 to 8-fold increase) depending on the membrane tension and applied technique and reduced uptake energy (reduction up to 80%) – manifest the crucial contribution of yet underrated lectin–glycolipid interactions in providing additional forces that assist membrane attachment and internalization of bacteria. This study also proves the advantages of combining force probing and synthetic biology for the mechanical characterization of host–pathogen interactions.

5. Experimental

5.1 Materials

1,2-Dioleoyl-*sn-glycero*-3-phosphocholine (DOPC) and cholesterol were purchased from Avanti Polar Lipids; Texas Red 1,2-dihexadecanoyl-*sn-glycero*-3-phosphaethanolamine (Tx-Red DHPE) from Life Technologies. The purified Gb3 extracted from red blood cells were supplied from Matreya. FSL-biotin was obtained from Sigma-Aldrich. Recombinant LecA was produced from *Escherichia coli* according to published procedures.[32,54] Sucrose was purchased from Carl Roth.

5.2 Lectin biotinylation

LecA was labelled with biotin NHS ester similar to a previously described protocol.[55,56] The binding of LecA after biotinylation to Gb3 receptors was examined by means of Gb3-functionalized vesicles (Fig. S5†).

5.3 AFM tip and OT bead functionalization

AFM probes (SD-sphere-cont-s and -m; Nanosensors) with a rounded hemisphere (*s*: 800 nm diameter and *m*: 2 μm) at the pyramid apex were purchased from Nanoandmore GmbH. They were first plasma cleaned and incubated in biotin-conjugated bovine serum albumin (biotin-BSA, 0.1 mg ml^{-1}) at 37 °C overnight. After three washes with PBS, they were incubated in a streptavidin solution (0.1 mg ml^{-1} in PBS) for 30 minutes. Subsequently, they were rinsed in PBS three times, incubated with biotinylated LecA (0.1 or 0.2 mg ml^{-1}) for 30 minutes and washed with PBS. For AFM experiments, biotinylated lipid species (FSL-biotin; 1 mol%) were incorporated into the GUV membrane in order to attach vesicles on a streptavidin-coated coverslip. According to confocal microscopy images of non-adherent (Fig. S6A†) and adherent (Fig. S6B†) GUVs on streptavidin-coated coverslips, it seemed that biotinylated lipids accumulate and stay at the bottom of the GUV in the contact area with the coverslip. Nevertheless, to minimize the undesired interactions between streptavidin molecules on the tip and biotinylated lipids in the GUV membrane, (any) free streptavidin molecules on the AFM tip were passivated by an additional incubation step of the functionalized tips with biotin (0.1 mg ml^{-1} in PBS; not shown in Fig. 1A) and finally washed with PBS. Except for the indicated temperature in the first functionalization step, all other steps have been performed at room temperature.

For the OT measurements, we used streptavidin-coated latex beads with a radius of 0.5 μm and functionalized them with biotinylated LecA following the supplier's protocol (Polyscience Inc.). Briefly, 50 μl of streptavidin-coated beads (particle concentration 1.25%) were centrifuged and gently washed 3 times using a PBS/BSA binding buffer at pH 7.4 and room temperature. Then, beads were resuspended in 1 ml of the binding buffer solution and subsequently incubated with 40 μl of biotinylated LecA solution (0.56 mg ml^{-1}). This is equivalent to 33 mg of LecA per mg of latex polymer, which resulted in LecA coverage of most of the latex beads. In order to verify the presence of LecA on the latex microsphere we incubated them with streptavidin Alexa Fluor 488 conjugate, which binds to the biotinylated LecA. The fluorescence signal of the beads was checked by confocal microscopy (Fig. S4†).

5.4 Bacterial attachment to the AFM tip

The *Pseudomonas aeruginosa* PAO1 wild-type strain (PAO1-WT) and the LecA-deletion mutant strain (PAO1-ΔLecA) were tagged with GFP as described in ref. 20. Biosafety regulations did not

permit working with live *Pseudomonas aeruginosa* PAO1 strain (biosafety level 2). We decided to use UV irradiation, which should inactivate the pathogens mainly by affecting nucleic acids and modifying the DNA,[57] as prior tests with formaldehyde fixation did not yield sufficient PAO1 inactivation (unpublished data) and strong chemical fixatives, such as glutaraldehyde, are supposed to have significant effects on the surface structure by crosslinking proteins or affecting the binding affinity of ligands.[58] Both strains were cultured overnight in Luria Broth (LB) medium in the presence of Gentamicin (60 μg ml^{-1}) at 37 °C to an OD of 0.6. The overnight cultures were pelleted and resuspended in PBS. Bacteria were diluted 1 : 500 in PBS and 1 ml was transferred to a plastic Petri dish, followed by UV treatment (UV-lamp at 254 nm, 188 μW cm^{-2}) for different time points (5 min to 20 min). Twenty microliters drops of diluted bacterial cultures before and after UV treatment were plated on LB agar plates and incubated overnight at 37 °C. The next day, colony forming units (CFUs) were counted and UV treatment efficiency was calculated. Based on the results, 20 min as the most efficient duration time was selected for AFM measurement.

The glass beads (10–15 μm; Kisker Biotech GmbH) were attached to tipless cantilevers (MLCT-O10, Bruker) using UV-curable glue.[59] Afterwards, bead-attached cantilevers were incubated in 0.1 w/v poly-L-lysin solution (Sigma-Aldrich) for 1 h at room temperature, washed with PBS and dried under a nitrogen stream. Using the AFM device, we caught a single inactivated bacterium (either PAO1-WT or PAO1-ΔLecA) with the coated bead. Afterwards, we transferred the obtained probe without dewetting the bacterium to a second chamber containing GUVs to perform the force spectroscopy measurements.

5.5 Substrate functionalization for AFM measurement

To prepare functionalized substrates, 24 mm diameter round glass coverslips were first sonicated in ethanol solution (50% v/v), then washed in distilled water and activated by sonication in sodium hydroxide solution (pH 12) to obtain a hydrophilic surface. The coverslips were rinsed and stored in distilled water for a few days. Prior to the experiment, the coverslip's surface was dried under a nitrogen stream and first passivated by a 0.1 mg ml^{-1} biotin–BSA solution for a minimum of two hours, and then incubated in a streptavidin solution (0.1 mg ml^{-1} in PBS) for 30 minutes. After washing with PBS, the streptavidin-coated coverslips were ready to use.

5.6 Liposome preparation

GUVs were prepared using the electroformation method.[60] Briefly, 10 μl of a 1 mg ml^{-1} lipid mixture dissolved in chloroform was spread on Indium-Tin-Oxide (ITO)-coated glass slides. The slides were placed in vacuum for several hours for complete evaporation of chloroform. A chamber was built between two slides around the lipid deposited area and filled with ~265 mOsm L^{-1} sucrose solution. Then, by applying an alternating electric field (1 V mm^{-1} field strength) to the chamber for 2–3 hours, GUVs were produced. For AFM measurements, the molar concentrations of the different GUV components were 30 mol% for cholesterol, 1 mol% for the biotinylated lipid (FSL-Biotin), 1 mol% for the glycosphingolipid Gb3 and 0.5 mol% for Tx-Red DHPE. The concentration of DOPC was adjusted to have in total 100 mol% dependent on the above mentioned components that have been used. For the low range of forces applied by OT, it was not necessary to adhere the GUVs by means of biotin–streptavidin linkage. Therefore, GUVs were prepared without the biotinylated lipids.

For the uptake experiments with OT, GUVs needed to possess much lower membrane tension in order to complete the bead internalization. Therefore, a certain membrane tension was chosen by imposing an average osmotic difference of 200 mOsm L^{-1} between the interior and exterior of the GUV.

5.7 AFM force spectroscopy measurements and analysis

All force measurements have been performed using a NanoWizard 3 and a CellHesion 200 (JPK BioAFM, Bruker Nano GmbH) integrated with an inverted Nikon Ti microscope equipped with a 40× water immersion objective and an Intensilight epifluorescence illuminator. While carefully avoiding lipid contamination on the AFM tips, they were placed on the top of the vesicles. Potential lipid contamination on the AFM tip was also checked after each recorded curve. The force measurements were performed with a velocity of 1 μm s^{-1} equivalent to approximate force rate of 10 nN s^{-1} and 200 nN s^{-1} for AFM measurements with bacteria and LecA-coated tips, respectively.

For the experimental setup with the bacteria, the length of the retraction part was recorded about 3 μm longer than the approach part to ensure the full separation of the AFM tip from the membrane.

The detachment forces, detachment works and unbinding steps were computed using JPK data processing software routines. To calculate the unbinding force and pulling lengths of the steps, we used step-fit operation, while keeping the same smoothing and significance parameters for all tested conditions.

5.8 Combined AFM and confocal laser scanning microscopy

The JPK Nanowizard 3 system was combined with a confocal microscope (Nikon Eclipse Ti-E inverted microscope equipped with a Nikon A1R confocal laser scanning system, 40× water immersion objective, NA = 1.25, laser line: 561 nm; Nikon Instruments). To create a deformation large enough to be detectable by confocal microscopy, we used AFM probes (SD-sphere-cont-m; Nanosensors) with a larger hemisphere (2 μm in diameter) and coated them with LecA (0.1 mg ml^{-1}) as described. The 3D image of GUVs was generated incrementally (0.2 μm steps) through the vesicle using a focal drive while the AFM force-indentation cycle was being performed.

5.9 Optical tweezers (OT)

The optical tweezers (OT) were used to trap and manipulate a dielectric particle in three dimensions through the sample and detect the changes in the particle position with nanometric precision.

The OT unit consisted of an infrared laser beam (Smart Laser Systems, λ = 1064 nm TEM00) focused by a water immersion objective lens (as the trapping lens) (UPLAPO Olympus 60×/IR, NA = 1.2). A latex bead in aqueous medium was trapped by the focused laser so that its position fluctuations b_i depend on the optical trap stiffness κ_i in the three directions (i = x, y, z). The exerted force on the particle was then given by F_i = κ_i × b_i. A noise eater (miniNE 2.1 TEM Messtechnik) was used to stabilize the laser power and to avoid undesired intensity fluctuations. The glass chamber was formed by two parallel coverslips separated by a plastic spacer of around ∼10 mm thickness. Two additional SiO_2 beads of 20 μm in diameter were used to aid the fixation of the vesicles at the bottom surface.

For the pulling experiments, the power (P) at the focal plane, inside the sample, was set to ∼50 mW producing a lateral trap stiffness of $\kappa_\perp$ = 90 pN μm^{-1}. For the uptake experiments, the transversal trap stiffness was varied from 5 pN μm^{-1} to 120 pN μm^{-1}.

The sample chamber was mounted on a piezoelectric stage (PZ, Piezosystem jena GmbH) for nanometric positioning control. The stage was moved with a controlled velocity (1 μms^{-1} and 0.1 μm s^{-1} for pulling and uptake experiments, respectively). A second objective lens named as detection lens (Achroplan 63×, NA = 0.95, Zeiss) collected and imaged at its back focal plane the interference pattern formed by the focused incoming light and the light scattered by the trapped particle. The interference pattern was detected by two quadrant photodiodes which recorded separately its lateral (x–y axis) and axial (z axis) changes at an acquisition rate of 1 MHz. From these interference patterns, we were able to accurately measure the changes in position of the trapped particle in 3D. Additionally, bright field and fluorescence microscopy techniques were integrated with the OT to optically monitor the GUVs.

5.10 Measurement of GUVs elastic properties

The surface membrane tension of vesicles $\sigma = \frac{F_t}{4\pi R_t}$ and the membrane bending rigidity $\kappa = \frac{F_t R_t}{2\pi}$ were calculated from the tether force F_t and the tether radius R_t. The value of F_t was obtained from the force–distance curves of uptake experiments as shown in Fig. 5A. The tether radius was taken from the fluorescence images by fitting a Gaussian function to the transversal intensity distribution of the formed tube.

Conflicts of interest

The authors declare no conflict of interest.

Acknowledgements

This work has been supported by the German Research Foundation grants [RO 4341/3-1, RTG 2202, EXC 294], the German Federal Ministry of Education and Research (BMBF) in the framework of the EU ERASynBio project SynGlycTis, and the University Freiburg “Strategiefonds”.

References

1 P. Schwille, *Science*, 2011, **333**, 1252–1254.
2 M. Weiss, J. P. Frohnmayer, L. T. Benk, B. Haller, J. Janiesch, T. Heitkamp, M. Börsch, R. B. Lira, R. Dimova, R. Lipowsky, E. Bodenschatz, J. Baret, T. Vidakovic-koch, K. Sundmacher, I. Platzman and J. P. Spatz, *Nat. Mater.*, 2018, **17**, 89–96.
3 D. Brüggemann, J. P. Frohnmayer and J. P. Spatz, *Beilstein J. Nanotechnol.*, 2014, **5**, 1193–1202.
4 S. F. Fenz and K. Sengupta, *Integr. Biol.*, 2012, **4**, 982–995.
5 J. P. Ribeiro, S. Villringer, D. Goyard, L. Coche-Guerente, M. Höferlin, O. Renaudet, W. Römer and A. Imberty, *Chem. Sci.*, 2018, **9**, 7634–7641.
6 S. Villringer, J. Madl, T. Sych, C. Manner, A. Imberty and W. Römer, *Sci. Rep.*, 2018, **8**, 1–11.
7 R. Omidvar and W. Römer, *Interface Focus*, 2019, **9**(2), DOI: 10.1098/rsfs.2018.0084.
8 M. Kaksonen and A. Roux, *Nat. Rev. Mol. Cell Biol.*, 2018, **19**, 313–326.
9 S. Aigal, J. Claudinon and W. Römer, *Biochim. Biophys. Acta, Mol. Cell Res.*, 2015, **1853**, 858–871.
10 H. Ewers and A. Helenius, *Cold Spring Harbor Perspect. Biol.*, 2011, **3**, 1–14.
11 T. Eierhoff, B. Stechmann and W. Römer, in *Molecular Regulation of Endocytosis*, ed. B. Ceresa, IntechOpen, London, 2012, pp. 249–276.
12 W. Römer, L. Berland, V. Chambon, K. Gaus, B. Windschiegl, D. Tenza, M. R. E. Aly, V. Fraisier, J.-C. Florent, D. Perrais, C. Lamaze, G. Raposo, C. Steinem, P. Sens, P. Bassereau and L. Johannes, *Nature*, 2007, **450**, 670–675.
13 M. Saleem, S. Morlot, A. Hohendahl, J. Manzi, M. Lenz and A. Roux, *Nat. Commun.*, 2015, **6**, DOI: 10.1038/ncomms7249.
14 A. Roux, G. Koster, M. Lenz, B. Sorre, J.-B. Manneville, P. Nassoy and P. Bassereau, *Proc. Natl. Acad. Sci. U. S. A.*, 2010, **107**, 4141–4146.
15 Z. Shi and T. Baumgart, *Nat. Commun.*, 2015, **6**, 1–8.
16 A. T. Hammond, F. A. Heberle, T. Baumgart, D. Holowka, B. Baird and G. W. Feigenson, *Proc. Natl. Acad. Sci. U. S. A.*, 2005, **98**, 9471–9473.
17 H. Ewers, W. Römer, A. E. Smith, K. Bacia, S. Dmitrieff, W. Chai, R. Mancini, J. Kartenbeck, V. Chambon, L. Berland, A. Oppenheim, G. Schwarzmann, T. Feizi, P. Schwille, P. Sens, A. Helenius and L. Johannes, *Nat. Cell Biol.*, 2010, **12**, 11–18.

18 G. E. Rydell, L. Svensson, G. Larson, L. Johannes and W. Römer, *Biochim. Biophys. Acta, Biomembr.*, 2013, **1828**, 1840–1845.
19 S. Wagner, D. Hauck, M. Hoffmann, R. Sommer, I. Joachim, R. Müller, A. Imberty, A. Varrot and A. Titz, *Angew. Chemie*, 2017, **129**, 16786–16791.
20 T. Eierhoff, B. Bastian, R. Thuenauer, J. Madl, A. Audfray, S. Aigal, S. Juillot, G. E. Rydell, S. Muller, S. de Bentzmann, A. Imberty, C. Fleck and W. Römer, *Proc. Natl. Acad. Sci. U. S. A.*, 2014, **111**, 12895–12900.
21 A. Novoa, T. Eierhoff, J. Topin, A. Varrot, S. Barluenga, A. Imberty, W. Römer and N. Winssinger, *Angew. Chem., Int. Ed.*, 2014, **53**, 8885–8889.
22 B. Maier, L. Potter, M. So, H. S. Seifert and M. P. Sheetz, *Proc. Natl. Acad. Sci. U. S. A.*, 2002, **99**, 16012–16017.
23 V. D. Gordon and L. Wang, *J. Cell Sci.*, 2019, **132**(7), DOI: 10.1242/jcs.227694.
24 N. C. Darnton and H. C. Berg, *Biophys. J.*, 2007, **92**, 2230–2236.
25 A. Persat, Y. F. Inclan, J. N. Engel, H. A. Stone and Z. Gitai, *Proc. Natl. Acad. Sci. U. S. A.*, 2015, **112**, 7563–7568.
26 S. Lu, M. Giuliani, H. Harvey, L. L. Burrows, R. A. Wickham and J. R. Dutcher, *Biophys. J.*, 2015, **108**, 2865–2875.
27 A. Beaussart, A. E. Baker, S. L. Kuchma, S. El-Kirat-Chatel, G. A. Otoole and Y. F. Dufrêne, *ACS Nano*, 2014, **8**, 10723–10733.
28 T. Sych, Y. Mély and W. Römer, *Philos. Trans. R. Soc., B*, 2018, **373**, 20170117.
29 N. C. Worstell, A. Singla, P. Saenkham, T. Galbadage, P. Sule, D. Lee, A. Mohr, J. S. Kwon, J. D. Cirillo and H. Wu, *Sci. Rep*, 2018, 1–11.
30 C. Chemani, A. Imberty, S. De Bentzmann, M. Pierre, M. Wimmerova, B. P. Guery and K. Faure, *Infect. Immun.*, 2009, **77**, 2065–2075.
31 L. Chaiet and F. J. Wolf, *Arch. Biochem. Biophys.*, 1964, **106**, 1–5.
32 B. Blanchard, A. Nurisso, E. Hollville, C. Tétaud, J. Wiels, M. Pokorná, M. Wimmerová, A. Varrot and A. Imberty, *J. Mol. Biol.*, 2008, **383**, 837–853.
33 J. Friedrichs, K. R. Legate, R. Schubert, M. Bharadwaj, C. Werner, D. J. Müller and M. Benoit, *Methods*, 2013, **60**, 169–178.
34 J. Helenius, C.-P. Heisenberg, H. E. Gaub and D. J. Muller, *J. Cell Sci.*, 2008, **121**, 1785–1791.
35 A. Janshoff and C. Steinem, *Biochim. Biophys. Acta, Mol. Cell Res.*, 2015, **1853**, 2977–2983.
36 A. Diz-Muñoz, D. A. Fletcher and O. D. Weiner, *Trends Cell Biol.*, 2013, **23**, 47–53.
37 E. Schäfer, M. Vache, T.-T. Kliesch and A. Janshoff, *Soft Matter*, 2015, **11**, 4487–4495.
38 A. Meinel, B. Tränkle, W. Römer and A. Rohrbach, *Soft Matter*, 2014, **10**, 3667–3678.
39 M. Deserno, *Phys. Rev. E: Stat., Nonlinear, Soft Matter Phys.*, 2004, **69**, 1–14.
40 D. Cuvelier, I. Derényi, P. Bassereau and P. Nassoy, *Biophys. J.*, 2005, **88**, 2714–2726.
41 T. S. Ursell, W. S. Klug and R. Phillips, *Proc. Natl. Acad. Sci. U. S. A.*, 2009, **106**, 13301–13306.
42 D. Opitz, M. Clausen and B. Maier, *ChemPhysChem*, 2009, **10**, 1614–1618.
43 Y. H. An and R. J. Friedman, *Handbook of bacterial adhesion: principles, methods, and applications*, Springer Science & Business Media, 2000, vol. 204.
44 K. A. Krogfelt, H. Bergmans and P. E. R. Klemm, *Infect. Immun.*, 1990, **58**, 1995–1998.
45 B. Pontes, P. Monzo and N. C. Gauthier, *Semin. Cell Dev. Biol.*, 2017, **71**, 30–41.
46 J. Pizarro-cerda and A. Ku, *Cold Spring Harbor. Perspect. Med.*, 2015, 1–18.
47 E. Veiga and P. Cossart, *Trends Cell Biol.*, 2006, **16**, 499–504.
48 E. A. Latomanski and H. J. Newton, *Microbiol. Mol. Biol. Rev.*, 2019, **83**, 1–25.
49 R. Ma and J. Berro, *PLoS Comput. Biol.*, 2018, **14**, 1–25.
50 W. K. den Otter and W. J. Briels, *Traffic*, 2011, **12**, 1407–1416.
51 M. M. Lacy, N. G. Ravindra, J. Berro, N. Haven, W. Haven, E. Biology, N. Haven and N. Haven, *FEBS Lett.*, 2018, **592**, 3586–3605.
52 E. Fischer-Friedrich, A. A. Hyman, F. Jülicher, D. J. Müller and J. Helenius, *Sci. Rep.*, 2014, **4**, 6213.
53 N. Minc, A. Boudaoud and F. Chang, *Curr. Biol.*, 2009, **19**, 1096–1101.
54 N. Kostlánová, E. P. Mitchell, H. Lortat-Jacob, S. Oscarson, M. Lahmann, N. Gilboa-Garber, G. Chambat, M. Wimmerová and A. Imberty, *J. Biol. Chem.*, 2005, **280**, 27839–27849.
55 S. K. Müller, I. Wilhelm, T. Schubert, K. Zittlau, A. Imberty, J. Madl, T. Eierhoff, R. Thuenauer and W. Römer, *Expert Opin. Drug Delivery*, 2017, **14**, 141–153.
56 W. Römer, L. L. Pontani, B. Sorre, C. Rentero, L. Berland, V. Chambon, C. Lamaze, P. Bassereau, C. Sykes, K. Gaus and L. Johannes, *Cell*, 2010, **140**, 540–553.
57 T. Dai, M. S. Vrahas, C. K. Murray and M. R. Hamblin, *Expert Rev. Anti.-Infect. Ther.*, 2012, **10**, 185–195.
58 I. W. McLean and P. K. Nakane, *J. Histochem. Cytochem.*, 1974, **22**, 1077–1083.
59 A. Beaussart, S. El-Kirat-Chatel, P. Herman, D. Alsteens, J. Mahillon, P. Hols and Y. F. Dufrêne, *Biophys. J.*, 2013, **104**, 1886–1892.
60 J. Madl, S. Villringer and W. Römer, in *Springer Protocols*, ed. A. K. Shukla, Springer Protocols Handbooks, 2016, pp. 17–36.

